On the apparent line-of-sight alignment of the peak X-ray intensity of the magnetosheath and the tangent to the magnetopause, as viewed by SMILE-SXI

Andrew Read*

Department of Physics & Astronomy, University of Leicester, Leicester, LE1 7RH, UK

Key Points:
- This work studies the hypothesis that, from a suitable point of view, the peak in the magnetosheath X-ray intensity can line up with the tangent to the magnetopause.
- Simulations of Soft X-ray Imager images and structures from the Solar wind Magnetosphere Ionosphere Link Explorer (SMILE) mission, using orbit and attitude data, are used to investigate this idea.
- Results for 3 years of the SMILE mission and for a range of solar wind densities and magnetopause models are presented.

Abstract: The Soft X-ray Imager (SXI) on board the Solar wind Magnetosphere Ionosphere Link Explorer (SMILE) spacecraft will be able to view the Earth's magnetosheath in soft X-rays. Simulated images of the X-ray emission visible from the position of SMILE are created for a range of solar wind densities by using 3 years of the SMILE mission orbit, together with models of the expected X-ray emissivity from the Earth's magnetosheath. Results from global magnetohydrodynamic simulations and a simple model for exospheric neutral densities are used to compare the locations of the lines of sight along which integrated soft X-ray intensities peak with the lines of sight lying tangent to surfaces (defined here to be the magnetopause) along which local soft X-ray intensities peak or exhibit their strongest gradients, or both, for strongly southward interplanetary magnetic field conditions when no depletion or low-latitude boundary layers are expected. Where, in the parameter space of the various times and seasons, orbital phases, solar wind conditions, and magnetopause models, the alignment of the X-ray emission peak with the magnetopause tangent is good, or is not, is presented. The main results are as follows. The spacecraft needs to be positioned well outside the magnetopause; low-altitude times near perigee are not good. In addition, there are seasonal aspects: dayside-apogee orbits are generally very good because the spacecraft travels out sunward at high altitude, but nightside-apogee orbits, behind the Earth, are bad because the spacecraft only rarely leaves the magnetopause. Dusk-apogee and dawn-apogee orbits are intermediate. Dayside-apogee orbits worsen slightly over the first three mission years, whereas nightside-apogee orbits improve slightly. Additionally, many more times of good agreement with the peak-to-tangent hypothesis occur when the solar wind is in a high-density state, as opposed to a low-density state. In a high-density state, the magnetopause is compressed, and the spacecraft is more often a good distance outside the magnetopause.

Keywords: X-rays; magnetosphere; magnetosheath; magnetopause; Solar wind Magnetosphere Ionosphere Link Explorer (SMILE); Earth; solar wind charge exchange

1. Introduction

The Solar wind Magnetosphere Ionosphere Link Explorer (SMILE; Branduardi-Raymont et al., 2018; Branduardi-Raymont and Wang C, 2022), a joint science mission between the European Space Agency (ESA) and the Chinese Academy of Sciences (CAS), was selected in November 2015, was adopted into ESA's Cosmic Vision Programme in March 2019, and is due for launch in March 2025. The SMILE spacecraft will be launched into a high-inclination,

highly elliptical orbit (~19 R_E [Earth radii] apogee, <2 R_E perigee), with a suite of instruments consisting of the Soft X-ray imager (SXI; Branduardi-Raymont and Wang C, 2022; Sembay et al., 2024), together with the Ultraviolet Imager (UVI), Light Ion Analyzer (LIA), and Magnetometer (see Branduardi-Raymont and Wang C, 2022). The SXI will use micropore optic technology and large-area X-ray-sensitive charge-coupled devices (CCDs) to provide spectroscopic imaging of the Earth's magnetosheath and cusp regions. The SXI will detect X-rays produced by the solar wind charge exchange (SWCX) process (e.g., see Robertson et al., 2006), where heavy ions within the solar wind collide with neutrals in the Earth's exosphere to produce soft X-rays. This process will enable the SXI to detect boundaries such as the subsolar magnetopause location

on relatively short timescales (a few minutes), depending on various parameters, including the solar wind ion flux, the neutral hydrogen density, and the ionized state of the solar wind.

A number of methods have been proposed to analyze the X-ray images produced by the SMILE-SXI and to extract information about the three-dimensional (3-D) magnetopause (e.g., Collier and Connor, 2018; Jorgensen et al., 2019; Sun TR et al., 2019, 2020; Connor et al., 2021; Samsonov et al., 2022a, b). For a number of these methods, a frequent assumption is that, from the point of view (POV) of the spacecraft or instrument (i.e., here, SMILE-SXI), the apparent position of the maximum in X-ray emissivity coincides (i.e., aligns) with the tangent to the magnetopause surface. This assumption is hereafter referred to in this study as "the hypothesis." This work aims to study, using the SMILE mission and orbit, together with up-to-date models of the magnetosheath and the magnetopause, how robust this hypothesis is for various scenarios (different solar wind densities, magnetopause definitions or models, and orbital positions during the year or mission). Were the hypothesis to be viable for even a subset of the various conditions and scenarios, it would be a useful tool.

Section 2 briefly describes the method used in this study and describes the computer simulation code that has been used. Section 3 describes the data that have been used: models of the magnetosheath X-ray emission and the magnetopause, and the orbit of the SMILE spacecraft during its mission. The results of the analysis are presented in Section 4 and are discussed in Section 5. Conclusions are presented in Section 6.

2. Method

The method used in this work is briefly described as follows (with additional details in the next sections): A "data cube" model is used to describe the X-ray emission in the magnetosheath and in the volume around the Earth at multiple 3-D points in space. An example of a data cube is shown in the left-hand panel of Figure 1. A second model, extracted directly from this X-ray emission cube, describes the magnetopause surface as a gridded structure in 3-D space, and an example of an extracted magnetopause model is shown in the right-hand panel of Figure 1. Computer code (described in the next section) is able to take these two models and simulate how both of them appear from the POV of the SMILE spacecraft and in the field of view (FOV) of the SXI instrument onboard SMILE, using the orbit data to position SMILE appropriately in the same 3-D space as the models. The peak in the X-ray emission and the tangent to the magnetopause can be identified, plotted, and overlaid in the FOV of the SXI, and their line-of-sight (LOS) coincidence, or not, can be examined and calculated for all points in time in the SMILE mission. The simulator code is described in the next subsection, and more information on the data models and the SMILE orbit and mission is given in the next sections.

It should be noted that only idealized scenarios are studied in this work. The X-ray images considered here are purely of the magnetosheath, and no background components, whether from the soft X-ray sky or from the instrument, are included. Additionally, the images are assumed to be as seen from the POV of SMILE, but not after having gone through the SXI; that is, no instrumental effects (e.g., the spectral response or electronic noise issues) are considered. The inclusion of background and instrumental effects is largely beyond the scope of the present study, although some discussion is presented in Section 5.3. As such, the results presented here are purely geometrical and can indeed be applica-
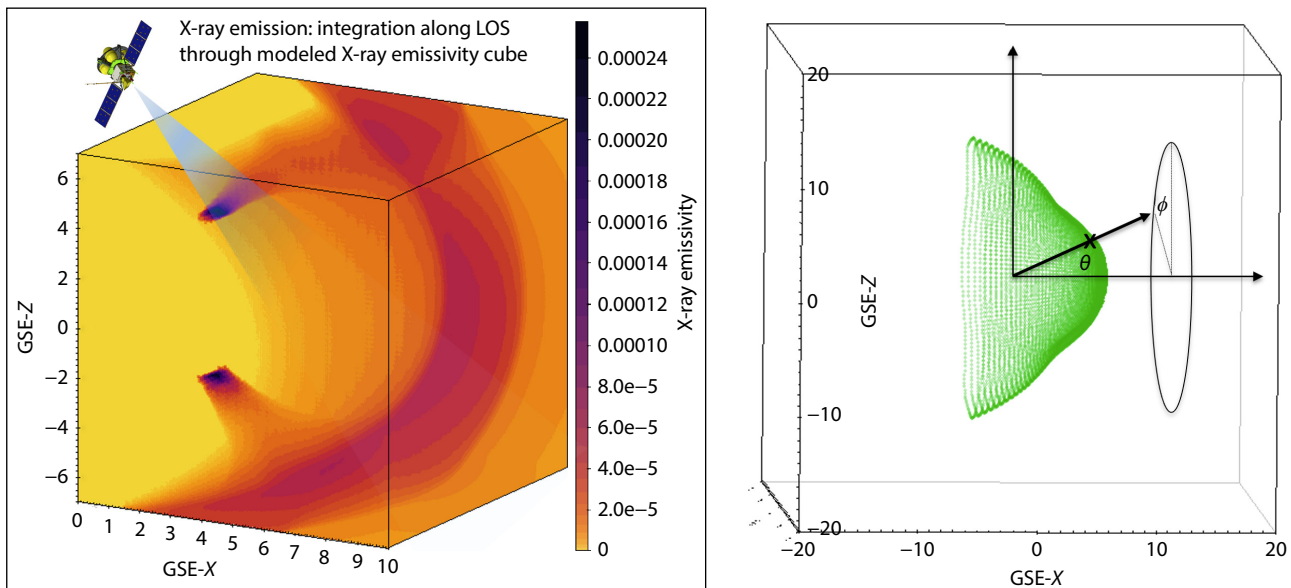
Figure 1.   (left) One of the X-ray emissivity cubes used in the work, showing the bow structure of the magnetosheath (dark red, at a large GSE-*X*) and the two very bright cusp regions nearer the Earth (very dark, at smaller GSE-*X*). A (not to scale) cartoon of the SMILE spacecraft is shown viewing the emission from high above the Earth. (right) An example of a magnetopause surface extracted from the X-ray emissivity cube (angles theta and phi are discussed in this article). The GSE-*X* and GSE-*Z* axes (units are Earth radii [R_E]) are marked in both panels, with GSE-*Y* pointing roughly into the page in both. The Earth sits at GSE-*X*, *Y*, *Z* = [0, 0, 0], the GSE-*X* axis points toward the Sun, and the GSE-*Z* axis lies perpendicular to the plane of the Earth's orbit around the Sun, with GSE-*Y* completing the orthogonal axes.

Read A.: Alignment of the magnetosheath X-ray peak with the magnetopause tangent as viewed by SMILE-SXI

ble to any suitably positioned, current or future observing instrument. It is the *inherent* offset between the peak in the magnetosheath X-ray emission and the tangent to the magnetopause, and the applicability of the idea that these two directions align, that is being studied and quantified here, over a range of solar wind conditions and viewing directions (here, from the SMILE orbit). Whether a particular instrument is able to measure the offset will depend on the characteristics and response of that instrument, although that is not within the scope of this work (but see Section 5.3 and Sembay et al., 2024, for an in-depth discussion of the SXI instrument and its response).

Throughout this work, the Geocentric Solar Ecliptic (GSE) coordinate system is used, with units in Earth radii. This system has the center of the Earth at [0, 0, 0], with the GSE-*X* axis pointing toward the Sun, and the GSE-*Z* axis perpendicular to the plane of the Earth's orbit around the Sun (positive GSE-*Z* extending above the northern hemisphere of the Earth). The GSE-*Y* axis completes the orthogonal *X*, *Y*, *Z* system and lies in the plane of the Earth's orbit around the Sun. This system is fixed with respect to the Earth–Sun line (the GSE-*X* axis) and is useful for specifying magnetospheric boundaries.

2.1 The SMILE Orbit and Viewing Simulator
The SMILE Orbit and Viewing (OV) simulator takes as input a number of positions in 3-D (GSE) space, namely, the spacecraft position, the pointing (aim) of the SMILE-SXI, and the positions and shapes or structures of various features of interest, such as the nose of the magnetopause; the magnetospheric cusps; the magnetopause itself, as well as the Earth, the Sun, and other objects (e.g., the Moon); and mathematical descriptions of any 3-D structures (e.g., complicated magnetopause and cusp surfaces). All this positional information can be static or time-evolving; for example, the spacecraft position and aimpoint can move, the nose can change position, and the cusps can change shape or size.

The simulator also takes as input the instrumental setup, namely, the geometry (e.g., optic FOV, CCD active FOVs, coverage and orientations, Sun and Earth baffles) and pointing of the SXI (the simulator is primarily built with the SXI observations as the focus) and the UVI (and the offset between the two instruments).

With this information, the simulator is able to calculate, purely geometrically, what is visible in the FOV of the SXI (and of the UVI). Plots showing the orbital information, and images of what is visible from the POV of the SXI are produced, either in a simple form, or in full information-rich animated detail. All this information can be collated over time (e.g., an orbit, a year, an entire mission) to build up observational efficiencies — that is, the percentage of time that a particular object (e.g., the nose) is visible in the SXI FOV and all other constraints are met (e.g., the SXI is on [the spacecraft is above a certain altitude] and no Sun- or Earth-baffle constraints are encountered). An important point regarding this work is that the simulator is able to take, as input, emission "cube" data (i.e., X-ray emissivity values as a function of the 3-D position in space) and use these to produce 2-D maps or images of the X-ray emission that would be visible at the (front of the) SXI, essentially by integrating along the lines of sight (LOS) from the spacecraft through

the emission cube, across a very large angle FOV (several tens of degrees square), at a fine (e.g., quarter-degree) angular resolution. These modules of the OV simulator code are also used within the SXI_SIM simulator code (see Section 5.3 and Sembay et al., 2024), which produces expected output images from the SXI instrument.

## 3. Data

3.1 The X-ray Emissivity Data Cubes
The X-ray emission in the magnetosheath and in the entire volume around the Earth is described in a data cube model, where the X-ray emissivity at multiple 3-D points in GSE space is stored. Specifically, the data cubes used in this study are the cases 1, 2, and 3 from Sun TR et al. (2019, 2021), and the details regarding these data cubes can be obtained from these references. An example of one of these data cubes is shown in the left-hand panel of Figure 1. These cubes were created using PPMLR-MHD (Piecewise Parabolic Method Lagrange Remap–Magnetohydrodynamics) code and have the following input solar wind parameters: velocity (in the minus *X* direction) 400 km s^{-1} ($V_y = V_z = 0$), interplanetary magnetic field (IMF) $B_z = -5$ nT ($B_x = B_y = 0$), and thermal pressure $p = 0.0125$ nPa for each of the three cases, but differing solar wind proton number densities of $D = 5$, 20, and 35 cm^{-3} at 30 R_E (GSE-*X*) in the solar wind. The three X-ray emissivity data cubes used here are referred to hereafter by these solar wind proton number densities: 5, 20, or 35 cm^{-3}. The number density of exospheric hydrogen was approximated by $N_H = n_0(10\ R_E/r)^3$ cm^{-3}, where $n_0 = 25$ was adopted, and a varying grid resolution was used, with a minimum value of 0.1 R_E near the subsolar point.

3.2 The Magnetopause Models
The Earth's magnetopause is the abrupt boundary between the Earth's magnetic field and the solar wind, and its location is determined by the dynamic pressure balance between the Earth's magnetic field and the solar wind (e.g., see Roelof and Sibeck, 1993; Shue et al., 1998).

An important point in the present study is that an attempt has been made to extract or form a "pseudo-magnetopause" surface model directly from the particular X-ray data cube model that is being considered. Hence, the 3-D X-ray emission and the pseudo-magnetopause surface (a single surface of zero "width" sitting within the 3-D space) that are being compared and positioned within each other come from the same source. We are not comparing apples with oranges by using an X-ray cube from one model or source and a magnetopause surface from a separate, different source, but instead, we are comparing apples with apples: both the X-ray emission and the pseudo-magnetopause surface used here come from the same source, from the same model.

The question then is how is the zero-width pseudo-magnetopause (hereafter, until the conclusions, "magnetopause") surface formed from the 3-D X-ray emissivity cube. If we extract from the 3-D cubes the X-ray emissivity values in a radial direction outward from the Earth in a direction that passes through the magnetosheath, we then get radial forms that look functionally similar to those in Figure 2, although the actual details do vary considerably
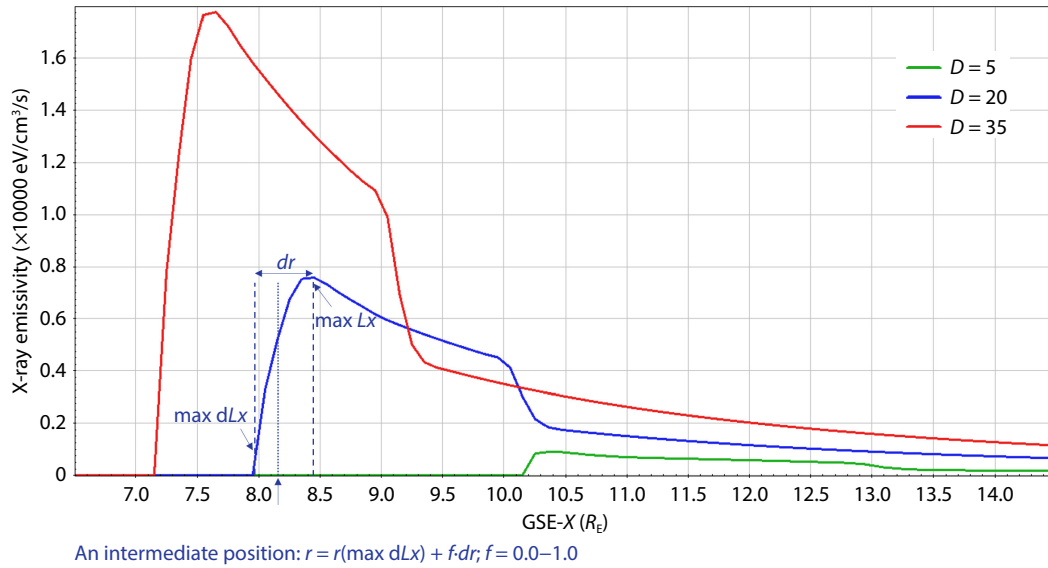
Figure 2. The X-ray emissivity (y-axis), extracted directly from each of the 3-D X-ray emissivity data cube models, along a single theta (angle away from the GSE-X axis)–phi (angle around the GSE-X axis) direction (here, along the GSE-X axis [theta = 0]), as a function of distance from the center of the Earth (x-axis). The max Lx and max dLx positions, a distance dr apart (see text), are shown for the $D = 20$ model (blue). The basic forms of the curves are roughly similar for each theta–phi direction that passes through the magnetosheath, with a near-zero base level, which rises sharply to a maximum before falling more slowly away. The particular shape, amplitude, and x-axis positions of the features and turning points, however, vary markedly with theta and phi, and with the data cube model. The $D = 35$ model (red) is the brightest and is compressed closest to the Earth, whereas the $D = 5$ model (green) is the faintest and peaks much farther out.

with the direction in space from the Earth outward. Here, the X-ray emissivity is near zero close to the Earth and remains close to zero for a few Earth radii inside the magnetopause, until at some radial distance from the Earth, it rapidly starts to increase, reaching a maximum a short distance farther out, before decreasing at a much shallower gradient than the steep increase prior to the maximum. We can define a number of (3-D) points in space along this radial straight line. The point at which the maximum X-ray emissivity ("max Lx") is observed is simple to define. Additionally, it is easy to calculate the point at which the maximum is reached in the gradient of the radial profile ("max dLx"). The magnetopause surface is therefore created by looping in 3-D space through two angles — theta, the angle away from the GSE-X axis, and phi, the angle around the GSE-X axis — and for each of these theta–phi directions, determining where (in 3-D space), on that particular radial line within the 3-D emissivity cube, (i) the emissivity is a maximum (max Lx), or (ii) the gradient of the emissivity is a maximum (max dLx). This then gives us a single grid-like surface (a 3-D X, Y, Z triple in space for each theta–phi direction) like that shown in the right-hand panel of Figure 1: one surface for max Lx, and another, separate surface (closer to the Earth for every theta–phi pair) for max dLx. These then represent two models (max Lx and max dLx) of the magnetopause surface, generated directly from each of the 3-D X-ray emissivity cubes.

Over the course of the study, it was discovered that a third magnetopause surface model was useful, one in between the max dLx and max Lx surfaces, and specifically at a quarter of the distance (for each theta–phi direction) between the max dLx and max Lx, namely, for f (as shown in Figure 2) equal to 0.25. This model is referred to in this work as the $f = 0.25$ model of the magnetopause surface.

3.3 The SMILE Orbit

For the purposes of this study, the orbit the SMILE spacecraft follows is the baseline orbit that was being adopted for the mission up until late 2021. At the time of this writing, a slightly different orbit was being adopted as the baseline orbit, and again, a slightly different orbit may well be the final orbit flown. The small changes between these orbits, however, make a negligible difference to the general results and conclusions of this work. The spacecraft orbit used here (launch November 2023) is a highly elliptical orbit, with an inclination of 70° and an argument of perigee of 287.5° that attains a maximum GSE-Z of slightly greater than ~18 R_E near apogee but an altitude below 1 R_E at perigee. Three years of the orbit are considered here: 2024, 2025, and 2026 (referred to here as year 1 [Y1], year 2 [Y2], and year 3 [Y3]). Note that the orbit currently being considered for the SMILE mission, with a proposed launch of November 2024, has a Y1 (2025) orbit that is almost identical to the Y1 (2024) orbit used in this study, and similarly on through the 3 years considered. Over the years, the orbit becomes more vertical in GSE space, with apogee being closest to the GSE-Z axis in Y3. Each year, the orbit reaches its maximum in positive GSE-Y (dusk-apogee, lying almost within the GSE-Y-Z plane) in late January ("Winter"), then reaches its maximum in positive GSE-X (dayside-apogee, lying in the GSE-X-Z plane) in late April ("Spring"), then reaches its maximum in negative GSE-Y (dawn-apogee, lying in the GSE-Y-Z plane) in late July ("Summer"), then reaches its maximum in negative GSE-X (nightside-apogee, lying in the GSE-X-Z plane) in late October ("Autumn"). Because the actual orbit that SMILE will eventually fly is not yet known, this connection between the month or season and location at apogee may not remain true. For this reason, and so this work can be related to other missions, the orbits are hereafter mainly referred

Read A.: Alignment of the magnetosheath X-ray peak with the magnetopause tangent as viewed by SMILE-SXI

to by location of apogee (dayside, dawn, nightside, dusk) rather than month or season.

Results using single-revolution (~50.3 h) orbits at these four points in the first year are presented first. The positions in GSE space of the SMILE spacecraft as a function of time for these four single-revolution orbits are listed in Table 1. Thereafter, results are presented using the entire full (>170 revolutions/year) spacecraft movement over each of the 3 years.

4. Results

We have then (i) 3-D models — the data cubes — of the X-ray emissivity in the magnetosheath and the region surrounding the Earth, (ii) 3-D (surface) models — grids of GSE-*X*, *Y*, *Z* values — of the magnetopause surface (generated directly from the 3-D X-ray emissivity cubes), and (iii) the SMILE orbit — the GSE position of the spacecraft through the mission. In addition, we have the attitude data for the mission, that is, where the SXI is pointing for each point in time in the mission.
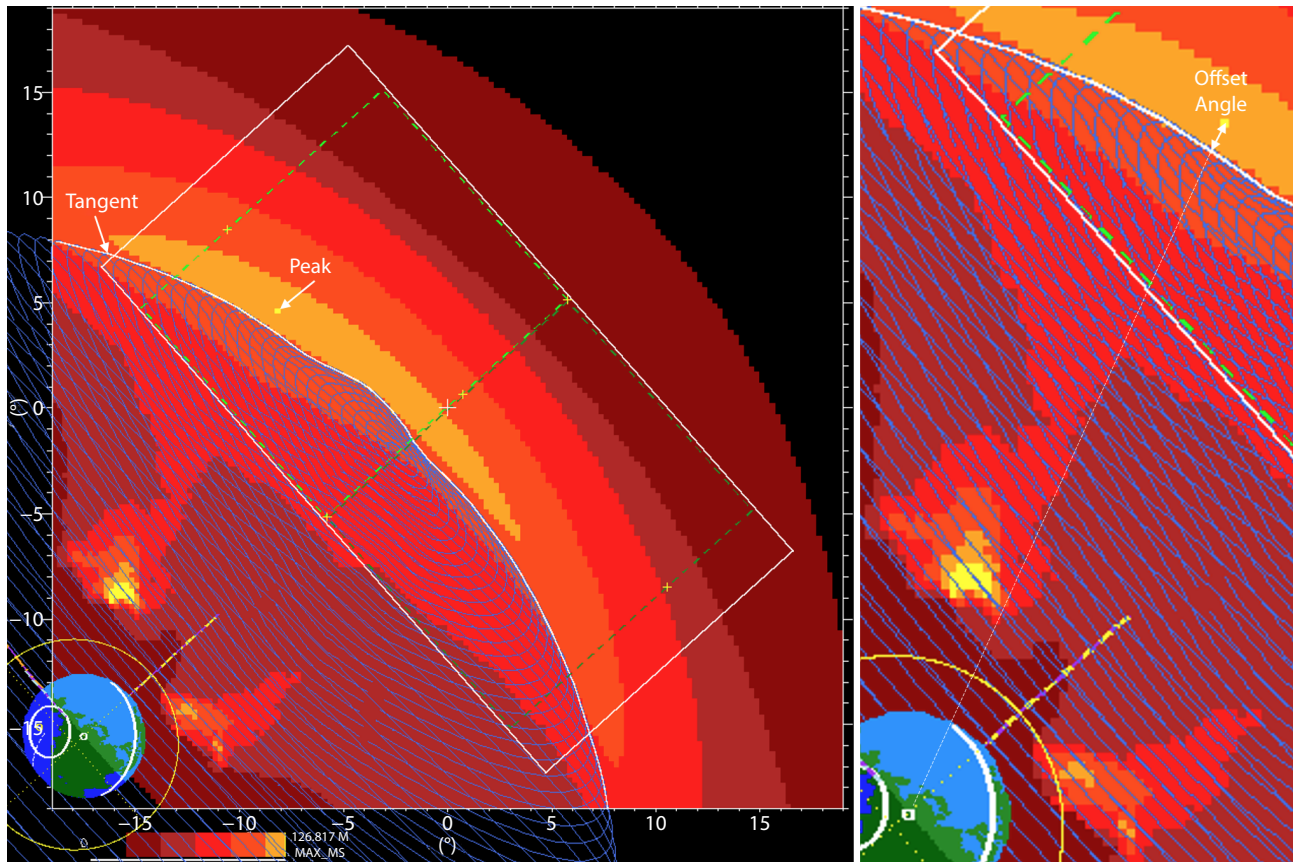
For a single instance in time in the mission, we can use the SMILE OV simulator to calculate and show what is visible within the SXI FOV from the POV of the SMILE spacecraft. An example of this is shown in Figure 3. Here, the large white rectangle shows the SXI FOV (with the active areas of the two SXI CCDs in light green and dark green). The SXI aimpoint is shown at the center of the FOV. The pixel image, following a black or dark red to bright yellow color table, shows the X-ray emission from the X-ray emissivity data cube, integrated along each LOS from the spacecraft out through the emissivity cube. The code is designed such that a single yellow pixel is selected (labeled "Peak") and highlighted in the magnetosheath where the actual peak in the magnetosheath X-ray emission is observed. In actuality, the brightest part of the magnetosheath X-ray emission forms a thin curve, parallel to the magnetopause tangent, but the single brightest point within that curve is highlighted in yellow and selected. (Brighter X-ray emission is seen from the cusps much closer to the Earth, these being, in this example, outside the SXI FOV.) The blue gridded structure shown is the magnetopause surface model (itself generated, remember, from the X-ray emissivity cube), with the individual *X*, *Y*, *Z* points in the magnetopause surface model joined with lines

to form a gridded surface. The simulator code is then able to select and highlight (here as the white curve at the outer edge of the blue gridded structure) the tangent to this magnetopause viewed from the spacecraft. The code then calculates the angular offset (in degrees) between the peak in the X-ray emission (the single yellow magnetosheath pixel) and the tangent to the magnetopause (the white curve) in a radial direction from the Earth, as shown in the zoomed-in right-hand panel of Figure 3. This calculated angular offset, referred to as "the offset," and whether it is positive (the X-ray peak is outside the tangent) or negative (the X-ray peak is inside the tangent) is the single variable that is used in the results that follow.

In the next sections, we look at how this offset varies along the four seasonal single-revolution orbits discussed earlier and throughout the full years of the mission. Before we do, though, it is worth noting a few general points. One important point is that to see the tangent to the magnetopause — to be able to test the validity of the hypothesis — one needs to be physically situated outside the magnetopause. At low spacecraft altitudes, before and after perigee, this is not true. Combined with this altitude effect, there are seasonal effects: dayside-apogee orbits extend at apogee out to positive GSE-*X*, between the Earth and the Sun, and the spacecraft is well outside the magnetopause, offering excellent views of the magnetopause tangent. Half-year later nightside-apogee orbits, however, extend toward negative GSE-*X* at apogee, behind (nightside of) the Earth. These orbits do not extend far outside the magnetopause at all, and they sometimes only barely cross the magnetopause. Listed in Table 2 are the approximate durations when the SMILE spacecraft is inside the magnetopause for the four single-revolution orbits and the three X-ray emissivity cubes used in this study. Note that each orbit has an approximate duration of 50.3 h, and for approximately 9.0 h, centered on perigee, and within the tabulated (in Table 2) inside-magnetopause periods, the spacecraft is below 50,000 km in altitude, and the SXI is nominally not observing. Because of uncertainties in determining the (pseudo-)magnetopause location purely from the X-ray data cube at positions far from the magnetopause nose, and particularly at negative GSE-*X* positions, simple magnetopause models following the parametrization of Shue et al. (1998) have been

Table 1.   The position in GSE-*X*, *Y*, *Z* space (units, R_E) of the SMILE spacecraft for the four single-revolution orbits used in this study, listed every 5 h after perigee (and therefore corresponding to the *x*-axis tick marks in Figures 4 to 8).

Time (h)	Dusk-apogee			Dayside-apogee			Dawn-apogee			Nightside-apogee		
	X	*Y*	*Z*	*X*	*Y*	*Z*	*X*	*Y*	*Z*	*X*	*Y*	*Z*
5	−0.16	−2.29	8.24	−3.04	0.16	7.71	0.17	3.59	7.72	4.25	−0.07	6.84
10	−0.30	0.79	13.91	−0.21	0.36	13.67	0.27	0.94	13.68	1.94	−0.27	13.20
15	−0.36	3.81	16.81	2.79	0.46	16.77	0.29	−2.01	16.82	−0.95	−0.40	16.62
20	−0.36	6.47	18.04	5.52	0.49	18.12	0.27	−4.78	18.20	−3.77	−0.46	18.19
25	−0.32	8.67	17.98	7.85	0.47	18.13	0.20	−7.20	18.21	−6.30	−0.47	18.33
30	−0.24	10.33	16.79	9.67	0.40	16.96	0.11	−9.13	16.99	−8.39	−0.42	17.21
35	−0.14	11.31	14.50	10.83	0.30	14.65	0.00	−10.40	14.59	−9.88	−0.34	14.86
40	−0.03	11.36	11.03	11.08	0.16	11.12	−0.12	−10.80	10.91	−10.50	−0.22	11.20
45	0.09	9.90	6.15	9.82	0.01	6.14	−0.21	−9.57	5.70	−9.56	−0.07	5.97

Read A.: Alignment of the magnetosheath X-ray peak with the magnetopause tangent as viewed by SMILE-SXI

Figure 3. An example of the SMILE OV simulator output, showing what is visible from the POV of the spacecraft (left shows a wide [38° × 38°] angular view; right shows a zoomed-in [13° × 25°] view of some important features). The SMILE-SXI optic FOV is shown by the large central white rectangular box (32.09° × 15.85°), with the active areas (open to the sky) of the two CCDs in light green and dark green. (The UVI FOV is shown by the smaller yellow circle [observing the Earth], and the Sun is off-image to the top right, with the Earth–Sun line [the GSE-X axis] here along the center line of the SXI FOV, between the two CCD active areas.) The SXI aimpoint is shown (white cross) at the center of the SXI FOV. The pixel image, following a black (lowest brightness), to red, to orange, to bright yellow (highest brightness) color table, shows the X-ray emission from the X-ray emissivity data cube, integrated along each LOS from the spacecraft out through the emissivity cube. The single yellow pixel highlighted (labeled "Peak") in the magnetosheath is where the actual peak in the magnetosheath X-ray emission is observed, with a value (in this example) of 126.8 keV cm^{-2} s^{-1} sr^{-1}. (The six colors below yellow in the color table peak at 0.18, 0.36, 0.54, 0.72, 0.90, and 0.99 times this value.) The blue gridded structure is the magnetopause surface model (generated from the X-ray emissivity cube). The white curve at the outer edge of the blue gridded structure (labeled "Tangent") shows the calculated tangent to this magnetopause from the POV of the spacecraft. The offset angle (see the right-hand zoomed-in image), between the peak in the X-ray emission (the single yellow magnetosheath pixel) and the tangent to the magnetopause (the white curve) in a radial direction from the Earth, is the single calculated variable that is used in the results. In this illustrative example, the peak lies 0.92° outside the tangent, and the spacecraft is positioned at GSE = [0.18, −7.84, 17.97] R_E.

Table 2. Approximate durations (in hours) when the SMILE spacecraft is inside the magnetopause for the four single-revolution orbits and the three X-ray emissivity data cubes used in this study.[a]

Cube number density (cm^{-3})	Dusk-apogee (h)	Dayside-apogee (h)	Dawn-apogee (h)	Nightside-apogee (h)
5	20.5	15.5	21.0	33.5
20	14.0	11.5	14.0	23.0
35	11.5	10.0	11.5	19.0

[a]Each orbit has an approximate duration of 50.3 h, and for approximately 9.0 h within the tabulated durations, the spacecraft is below 50,000 km in altitude and the SXI is nominally not observing.

constructed that closely fit the $f = 0.25$ magnetopause models for the three X-ray emissivity cubes (5, 20, and 35 cm^{-3}) considered. The approximate durations tabulated in Table 2 have then been calculated using these Shue models and the four single-revolution orbits.

To maximize the times when the spacecraft is outside the magnetopause, it makes sense, initially, to study the smallest magnetopause case, that is, the highest density solar wind case, the $D =$

Read A.: Alignment of the magnetosheath X-ray peak with the magnetopause tangent as viewed by SMILE-SXI

35 cm^{-3} case, because here the magnetosheath and the associated magnetopause are compressed inward, closer to the Earth than in the $D = 5$ or $D = 20$ cases.
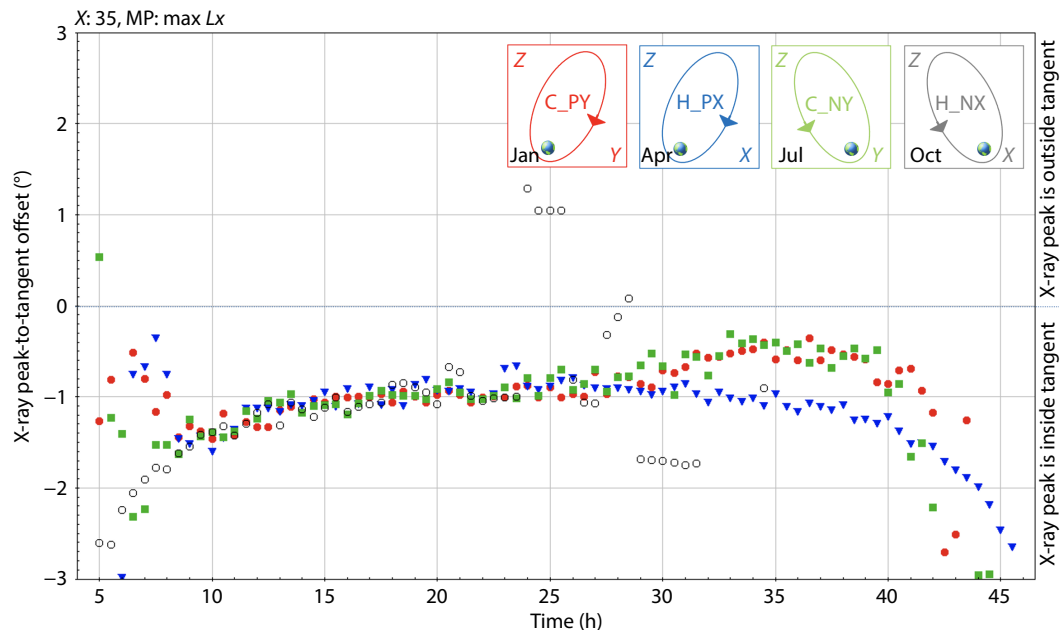
4.1 Results Using Single-Revolution Seasonal Orbits

The OV simulator was run using the four seasonal single-revolution orbits from Y1, each of approximately 50.3 h duration and stretching from perigee, through apogee, to next perigee, from late January (dusk-apogee), April (dayside-apogee), July (dawn-apogee), and October (nightside-apogee). The X-ray peak-to-tangent angular offset was calculated at half-hourly intervals, using the $D = 35$ cm^{-3} X-ray emissivity data cube and, first, using the max Lx magnetopause model (generated directly from this cube). These values are plotted as a function of time in Figure 4. Simple schematics of the four orbits are shown as insets in the figure.

Many details are evident from the figure. It is important to note that (almost) all the points and the general trends of the four seasonal cases lie significantly below the offset = 0 line, that is, the offset values are negative, meaning the X-ray peak is observed to lie inside (nearer the Earth) the tangent to the magnetopause. For the hypothesis (that the apparent maximum in the X-ray emissivity aligns with the tangent to the magnetopause surface) to be true requires that the points in Figure 4 lie close to or on the offset = 0 line, but here, for the data and models used in this first case, they do not.

Looking at the individual orbits, we see some similarities and differences. The red and green points, for instance, behave very

similarly. This is expected because these points correspond to the dusk-apogee (red) and the dawn-apogee (green) orbits, which are mirrors of each other. The dusk-apogee orbit extends to positive GSE-Y at apogee, and the dawn-apogee orbit extends to negative GSE-Y at apogee, and both orbits lie almost within the GSE-Y-Z plane (close to GSE-X ~0). Hence their views of the magnetosheath and the magnetopause are symmetrically similar around these orbits. The red and green curves appear to become chaotic (i.e., the point-to-point variation becomes large) at the start and end of the orbits. This is understandable in terms of the spacecraft traveling close to the Earth during these times and very close to, or often inside, the magnetopause, where measuring any tangent may become difficult, impossible, or meaningless. The blue (dayside-apogee) and gray (nightside-apogee) orbits are very different. The dayside-apogee orbit, like the orbits 3 months before (red) and after (green), appears chaotic at the start, as the spacecraft is coming out around the back of the Earth, and is close to or inside the magnetopause during these times. For the rest of the blue dayside-apogee orbit, because it extends out to positive GSE-X at apogee, it is fully well outside the magnetopause all the time and offers excellent views of the magnetopause and magnetosheath. The nightside-apogee (gray) orbit, however, although it starts well as it comes out in front of the Earth, it quickly, near apogee (at the midpoint of the x-axis), becomes chaotic, with further meaningless values outside the y-axis range. This is because this orbit extends to negative GSE-X at apogee, so it dips quickly inside the magnetopause. It also, after apogee, returns behind the Earth and has no view toward the nose of the magnetosheath because it would be viewing too closely to the Sun.

Figure 4. The X-ray peak-to-tangent angular offset (y-axis, degrees) versus time (x-axis, hours), using the $D = 35$ X-ray emissivity data cube and the corresponding max Lx magnetopause (MP) model, for four single-revolution seasonal year 1 (Y1) orbits: dusk-apogee (red filled circles, January), dayside-apogee (blue triangles, April), dawn-apogee (green squares, July), nightside-apogee (gray open circles, October). The orbital GSE positions are given in Table 1, and simple schematics of the four orbits in GSE space are shown in the insets. Positive offset values indicate that the peak in the X-ray emission is outside the tangent to the magnetopause, and negative offset values indicate that it is inside. The x-axis runs from 4 h after perigee, through apogee at the midpoint of the x-axis, to 4 h before the next perigee (thus spanning the approximate time when SMILE is above 50,000 km in altitude and the SXI is nominally observing).

Read A.: Alignment of the magnetosheath X-ray peak with the magnetopause tangent as viewed by SMILE-SXI

Usage of the max *Lx* magnetopause model therefore, during times of satisfactory to good viewing conditions, leads to consistently negative peak-to-tangent offset values, that is, the X-ray peak is always seen to lie inside the tangent to the magnetopause.

We then compare usage of the max d*Lx* magnetopause model. Figure 5 shows the results when this magnetopause model is used. Nothing else is changed: the *D* = 35 X-ray emissivity cube is again used, and the orbits are still the same. Here, though, we see that the offset values are now consistently positive, that is, the X-ray peak is now seen to lie outside the tangent to the magnetopause. In addition, the general trends are closer to the offset = 0 line, meaning the max d*Lx* magnetopause model is a better model than the max *Lx* model in terms of satisfying the hypothesis, but we have overshot a "best" magnetopause model when going from max *Lx* to max d*Lx*. Again, similar trends and constraints are seen: the dayside-apogee orbit is again good for almost all the orbit, the dusk-apogee and dawn-apogee orbits mirror each other again but again suffer toward the end of the orbits, and again, the nightside-apogee orbit fares badly for much of the orbit.
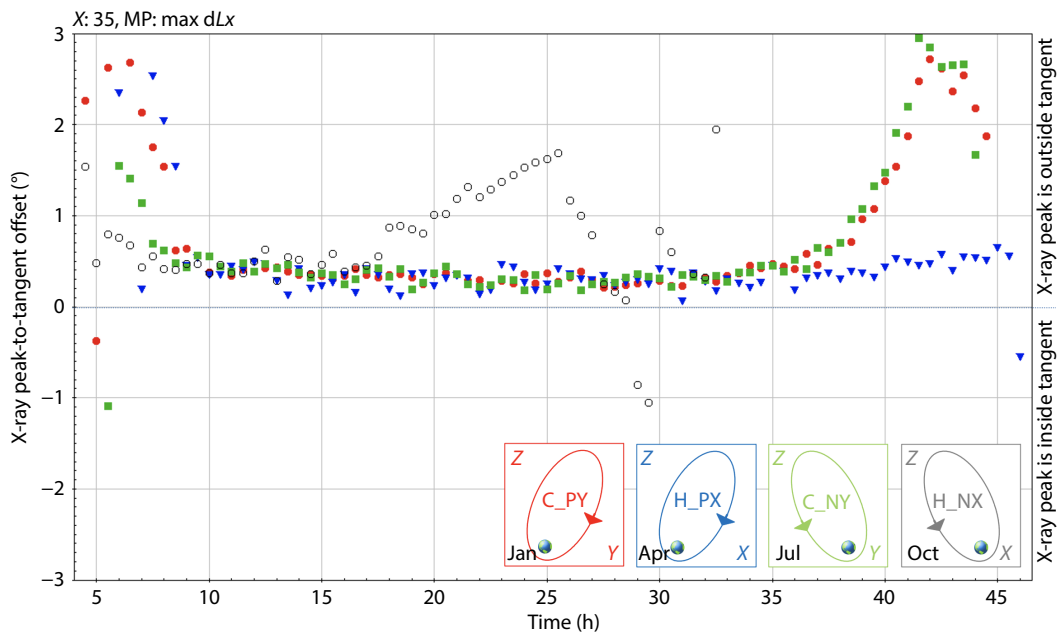
The results obtained using the max *Lx* and the max d*Lx* magnetopause models suggest that a better model than either is one lying in between the two, and closer to the max d*Lx* model than to the max *Lx* model, hence the *f* = 0.25 magnetopause model described earlier. The results using this model (as well as the same X-ray emissivity data cube [*D* = 35] and the same four orbits as previously) are shown in Figure 6. This model bears many similarities to the previous max d*Lx* results, but there is a shift downward such that the general trends, during times of good visibility and being outside the magnetopause, are more centered around the offset = 0 line. The results are a little noisier than as seen previously. This is because, in the construction of the *f* = 0.25 magnetopause model, for a particular theta–phi direction, both a valid (3-D, *X-Y-Z*) point at max d*Lx* and a valid point at max *Lx* need to

be found to calculate a point a quarter of the distance between the two. For the max d*Lx* or the max *Lx* model, the requirement is that only the one point be found. Hence, the *f* = 0.25 magnetopause gridded structure is slightly more sparsely populated than the other two models, and the calculation of the offset angle is consequently slightly noisier. That said, usage of the *f* = 0.25 magnetopause model yields results that are generally closest to the offset = 0 line, meaning it is the model that best (of the three) satisfies the hypothesis.

For the results presented here, we are calculating and plotting an offset *angle* (in degrees). This angle can be converted to a physical distance (in Earth radii), although it is not a simple conversion because the peak in the X-ray intensity comes not from a single point in space, but is integrated along a particular direction, and the tangent lies at varying distances from the nose of the magnetopause. Only when the spacecraft has the same GSE *X*-position as the nose does the tangent touch the nose. These complexities notwithstanding, an approximate conversion of the *f* = 0.25 angular results of Figure 6 to a distance, assuming the offset to be at a distance corresponding to the nose of the magnetopause, is shown in Figure 7. This conversion has the general effect of lessening, relatively, the departures from offset = 0 that are seen at the start and end of the orbits because the spacecraft is usually closer to the nose of the magnetopause at these times (and an angular offset then corresponds to a smaller physical offset distance), compared with times closer to apogee.
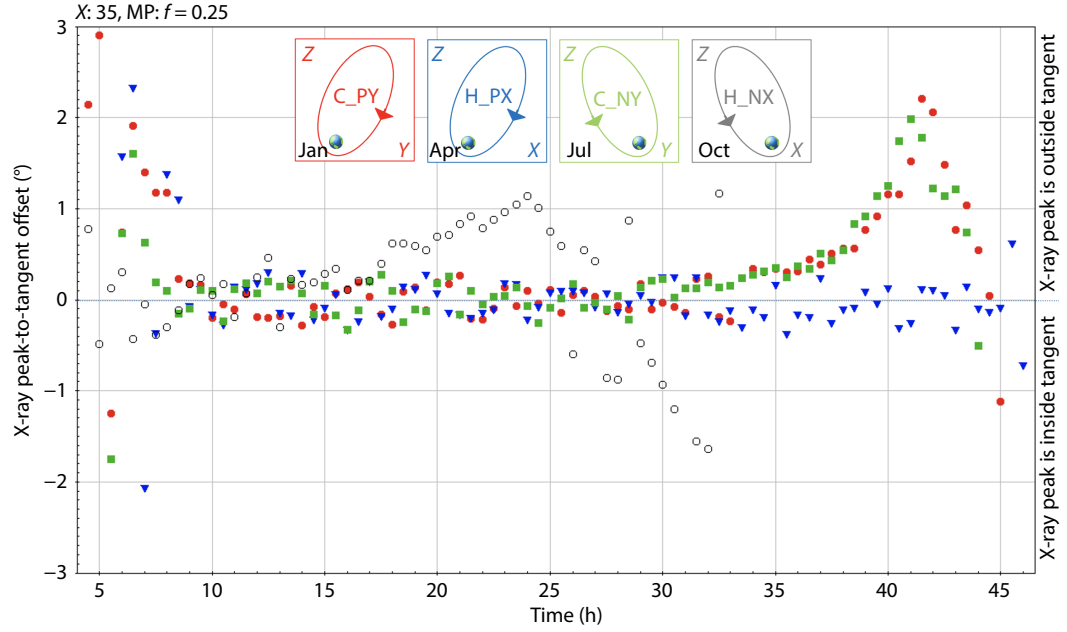
4.2 Results Using Whole-Year Orbits
We now extend the analysis to cover the full duration of all the years Y1, Y2, and Y3, and using the lower density *D* = 5 cm^{-3} and *D* = 20 cm^{-3} cases as well. Large yearlong simulations were run, again using the SMILE OV simulator to calculate and show what is visible in the SXI FOV from the POV of the SMILE spacecraft, and then to calculate the X-ray peak-to-tangent offset angle for various
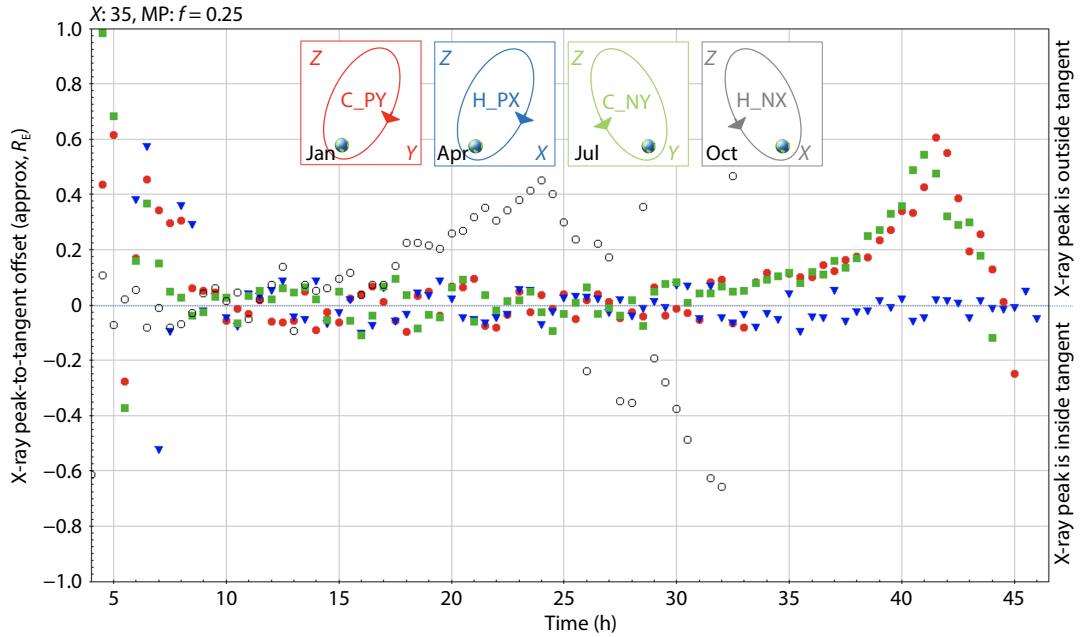

Figure 5. As for Figure 4 but using the max d*Lx* magnetopause (MP) model.

Read A.: Alignment of the magnetosheath X-ray peak with the magnetopause tangent as viewed by SMILE-SXI

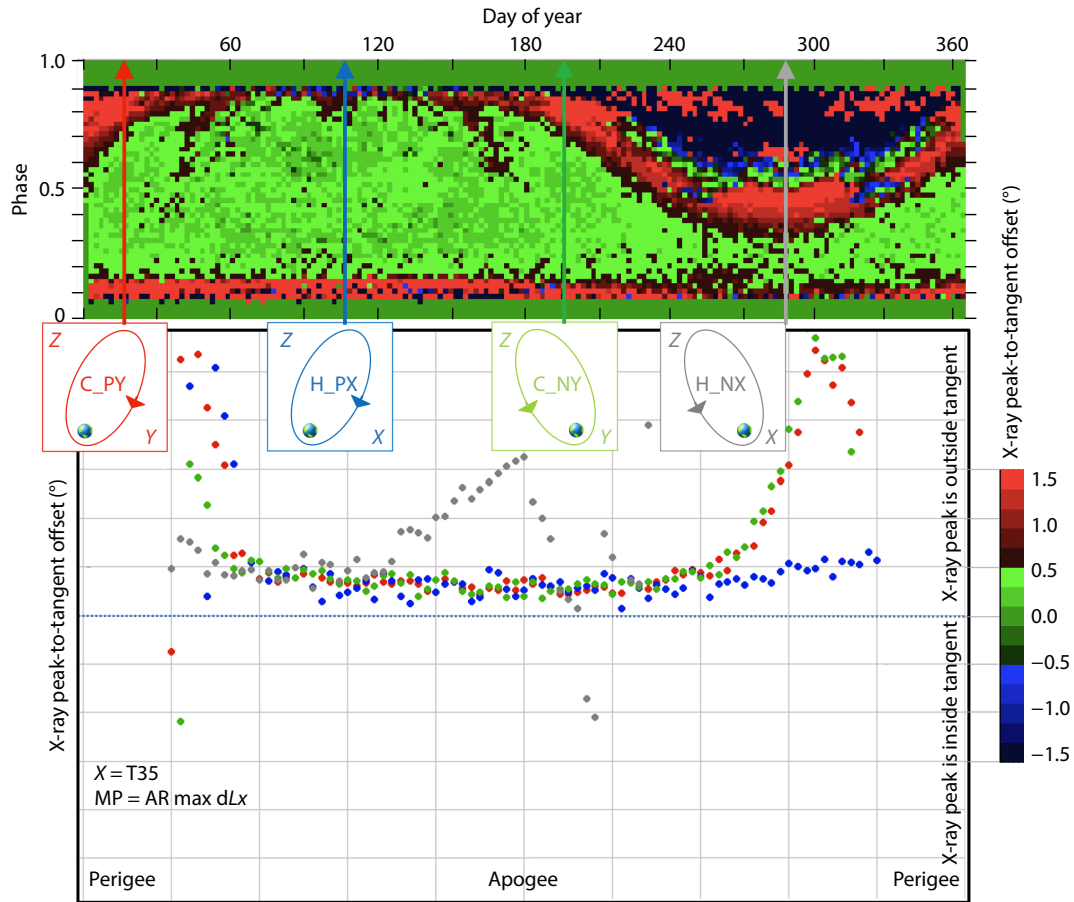**Figure 6**. As for Figure 4 but using the $f = 0.25$ magnetopause (MP) model.

Figure 7. As for Figure 4 but using the $f = 0.25$ magnetopause (MP) model, and here converting the y-axis offset values from an angle to an approximate physical distance (in R_E), assuming the offset to be at a distance corresponding to the position of the nose of the magnetopause.

combinations of year (Y1, Y2, or Y3), X-ray emissivity data cube model ($D = 5$, 20, or 35 cm^{-3}), and magnetopause model (max Lx, max dLx, or $f = 0.25$), these generated directly from the specific X-ray emissivity data cube. To reduce the very long run time of these simulations, a time step of one hour (as opposed to a half hour previously) was used, although this still resulted in 8760 simulated frames (time steps) per yearly run.

Here, we use a "phase–year" diagram (see Figure 8) to plot the calculated offset angle as a colored pixel (with the color denoting the offset angle) in a 2-D array or map, with the x-axis (year) of the map running from January 1 to December 31 and the y-axis

(orbital phase) running from perigee (bottom), through apogee (halfway up), to next perigee (top). This allows the results (the offset angle) for each time step in the year to be displayed as a colored pixel in the x-y plane of the phase–year diagram. The color bar is such that "good" values of the X-ray peak-to-tangent offset angle, here defined as running from −0.5° to +0.5°, are colored green, whereas when the X-ray peak is far outside the tangent (offset greater than +0.5°), they are colored red, and when the X-ray peak is far inside the tangent (offset less than −0.5°), they are colored blue.

Figure 8 makes use of the $D = 35$ cm^{-3} data cube and the max dLx

Read A.: Alignment of the magnetosheath X-ray peak with the magnetopause tangent as viewed by SMILE-SXI

Figure 8. The bottom panel shows the results presented previously in Figure 5 for the four seasonal single-revolution orbits and using the $D = 35$ cm^{-3} X-ray emissivity cube, and the max dLx magnetopause (MP) model, generated directly from the cube. A color bar is shown to the right of this, running from dark blue (offset angle = −1.5) to light red (offset angle = +1.5), and this color coding is used in the upper panel, which shows the results for the same input emissivity and magnetopause models, but for the whole year in a "phase–year" plot. In this upper panel, the x-axis (year) runs from January 1 to December 31 and the y-axis (orbital phase) runs from perigee (bottom), through apogee (halfway up), to next perigee (top), and the offset angle calculated for each phase point in each orbit is plotted as a colored pixel, the offset angle value given by the color table. The pixels where the results for the four single-revolution orbits appear in the phase–year plot are indicated by the vertical arrows. The blank green regions to the top and bottom of the phase–year plot indicate when the spacecraft is below 50,000 km and the SXI is nominally not observing.

magnetopause model generated from that cube. The results for the single-revolution seasonal orbits for these models, previously plotted in Figure 5 and plotted in the lower panel of Figure 8, are situated in the upper panel of Figure 8 under the vertical arrows. One can see that the profiles of the red-arrow (dusk-apogee) and green-arrow (dawn-apogee) orbits appear to be very similar, with the X-ray peak starting far outside the tangent (red), then becoming good (green) through most of the orbit before drifting far outside the tangent (red) again toward the end of the orbit. The blue-arrow (dayside-apogee) orbit is very good, with very short periods at the start and end of the orbit when the X-ray peak is far outside the tangent, but the large majority of the orbit is good (green). The gray-arrow (nightside-apogee) orbit is, conversely, very bad, with only a short period of the orbit near the start when anything useful is seen. This behavior has been described earlier, but now in the 2-D phase–year plot, the results for the entire year can be seen. For the entire year, the fact that the large green central region is (very) light green indicates that the X-ray peak is,

even when good, still somewhat outside the tangent to the magnetopause for the models used here.

The phase–year plot (top panel in Figure 8), which uses the max dLx magnetopause model, is plotted together with the calculated phase–year plots that use the $f = 0.25$ and the max Lx magnetopause models (Figure 9). These results all use the $D = 35$ cm^{-3} data cube and are for Y1, so Figure 9 shows the effects of varying only the magnetopause model. As shown before, though, now for all orbits and times within Y1, the $f = 0.25$ magnetopause model fares best in terms of satisfying the peak–tangent hypothesis, with much of the mid- to high-altitude points colored mid-green (i.e., offset ~0). The max dLx model is a little worse (light green and very light green), and the max Lx is poor, with the large dark blue regions indicating offset angles of −1° and worse. In addition, very apparent in these plots are the strong effects of the orbit going significantly behind the Earth during the pre-perigee times in and around Autumn (nightside-apogee). Here, the spacecraft dips repeatedly inside the magnetopause, making tangential calcula-
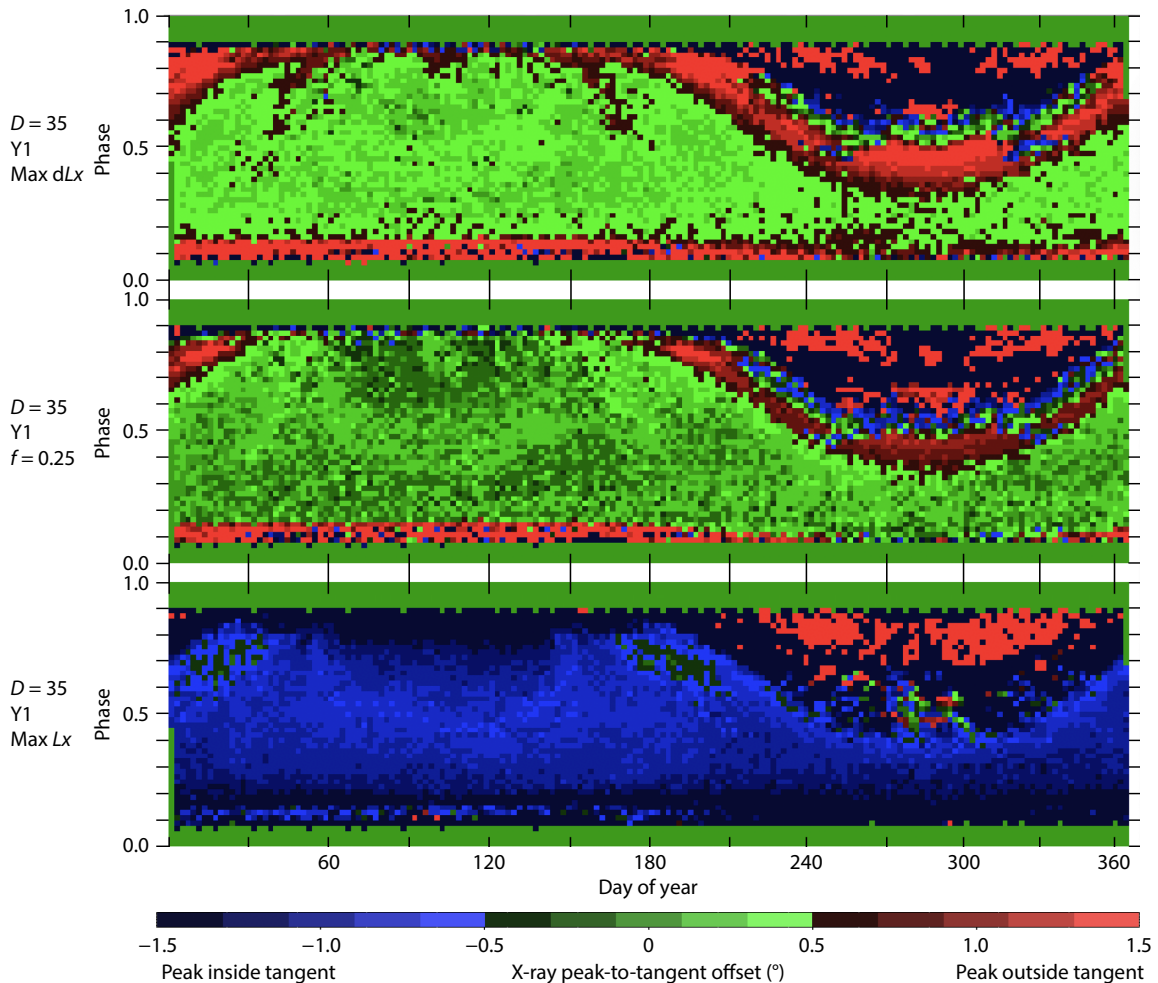
Figure 9. Three phase–year plots of the calculated X-ray peak-to-tangent offset angle (see color bar at the base) in a 2-D array, the x-axis (year) running from January 1 (left) to December 31 (right), and the y-axes (orbital phase) running from perigee (bottom) through apogee (halfway up) to next perigee (top). The three panels shown are for year 1 (Y1) and the $D = 35$ cm^{-3} X-ray emissivity cube, and using the (top panel) max dLx, (middle panel) $f = 0.25$, and (bottom panel) max Lx magnetopause models, each generated from the $D = 35$ cm^{-3} X-ray emissivity cube. The blank green regions to the top and bottom of each panel indicate when the spacecraft is below 50,000 km and the SXI is nominally not observing.
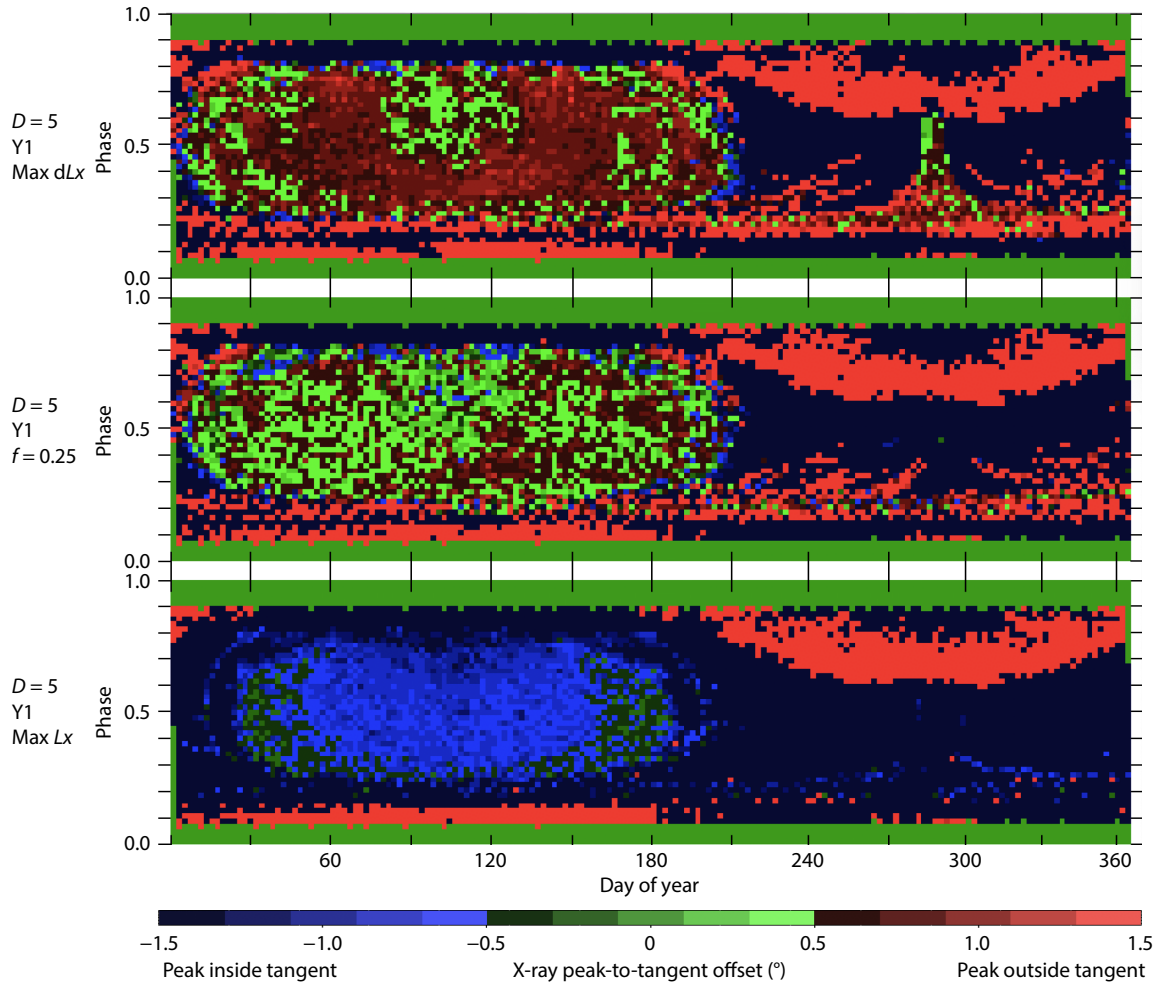
tions impossible, and the nose of the magnetopause becomes impossible to view because of Sun constraints.

Figure 10 shows the equivalent phase–year results, varying the magnetopause model for Y1, but for $D = 5$ cm^{-3}, the lowest density case. Here, the results are much worse than for the $D = 35$ cm^{-3} case, with the only satisfactory to good results obtainable by using the $f = 0.25$ magnetopause model and only significantly away from perigee and only in the first half of the year. All this is because, in this low-density case, the magnetopause surface is the farthest out — it is the most extended — and the spacecraft is inside or close to the magnetopause much more often than for the high-density case.

To explore this further, Figure 11 shows phase–year plots for Y1 and using the best magnetopause model — the $f = 0.25$ model — for the three solar wind densities considered here, $D = 5$, 20, and 35 cm^{-3}. The results are poor for the lowest density case, where the magnetopause is large and closest to the spacecraft orbit. The results are best for the highest density case, where the magnetopause is compressed inward and is at its smallest, and where

the spacecraft is well above the magnetopause many more times and is able to have clear views.

Having established that we can obtain good results that satisfy the peak–tangent hypothesis, but only away from perigee, and the best results using the $f = 0.25$ magnetopause model, but only when the solar wind is in a high-density state, then we can look at how these results vary with the year of the mission. Figure 12 shows the phase–year results for the high-density, $D = 35$ cm^{-3}, case and using the $f = 0.25$ magnetopause model for Y1, Y2, and Y3. Here, we see the effects of the orbit evolving during the mission. During Y1, apogee is reached a significant distance (~5 R_E) away from the GSE-Z axis. By Y3, however, the orbit becomes more vertical in GSE space such that apogee is almost on the GSE-Z axis. This result explains how the large Autumnal pre-perigee problem area visible in Y1 evolves into two half-sized problem areas, one in Autumn pre-perigee and the other in Spring post-perigee. In Y3, Autumn orbits effectively follow the same paths in GSE space as Spring orbits, but in an opposite direction (and similarly for Winter–Summer). Apart from this geometrical difference, there is very little difference between the years. The $f = 0.25$

Read A.: Alignment of the magnetosheath X-ray peak with the magnetopause tangent as viewed by SMILE-SXI

Figure 10. The same as for Figure 9, but for year 1 (Y1) and the $D = 5$ cm^{-3} X-ray emissivity cube, and using the (top panel) max dLx, (middle panel) $f = 0.25$, and (bottom panel) max Lx magnetopause models, each generated from the $D = 5$ cm^{-3} X-ray emissivity cube.

model fares equally well across the years when the conditions are good enough to provide favorable views.

We can assign a value to each of the yearlong simulations performed by calculating, for each case studied, the percentage of time in the year when the SXI is on, when it is in nominal viewing mode, and when the offset angle is good (i.e., it lies between −0.5° and 0.5°) or is excellent (i.e., it lies between −0.1° and 0.1°). These numbers are tabulated in Table 3 (good) and Table 4 (excellent).

The same trends are evident in the tables. The best results, in terms of satisfying the peak–tangent hypothesis, are obtained when the solar wind is in a high-density state. The $f = 0.25$ model is the best of the magnetopause models used, with the max dLx model faring better than the poor max Lx model and with no substantial change from year to year.

In combination with these results, the percentage of the year when the solar wind conditions assumed in this study might be met can be estimated by using the online service at omniweb.gsfc. nasa.gov to look at previous years. Listed in Table 5 are the observed percentages of year for various combinations of IMF B_Z, solar wind velocity, and solar wind density for the equivalent 3 years studied here, from solar cycle 23 (years 2000–2002) and (the weaker, certainly in the first 2 years) solar cycle 24 (years

2013–2015). Rather low percentages are seen if the emissivity cube model values ($B_Z = -5$ nT, $V_{SW} = 400$ km s^{-1}, $D_{SW} = 5$, 20, 35 cm^{-3}) are taken as restrictive limits (rows 1–3 in Table 5), but larger percentages are often obtained if the various model values are more representative of a range of values (rows 4–12; see footnote).

At the time of writing, the three emissivity cubes used were the only data cubes from Sun TR et al. (2019) that were made available for this study. These data cubes have a southward IMF orientation, whereas an equatorial orientation is more typical of the IMF. (The IMF also has an equally northward orientation for a similar duration.) Again according to omniweb.gsfc.nasa.gov, the percentage of year when B_Z was observed to be less than −5 was 9%–10% during 2000–2002 (solar cycle 23) and 6%–8% during 2013–2015 (solar cycle 24). The corresponding $B_Z < -2.5$ values were 23%–26% (2000–2002) and 18%–23% (2013–2015).

5. Discussion

5.1 Validity of the Hypothesis
The results presented here show that the hypothesis — that from the POV of the spacecraft, the peak in the magnetosheath X-ray emission aligns with the tangent to the magnetopause — can

Read A.: Alignment of the magnetosheath X-ray peak with the magnetopause tangent as viewed by SMILE-SXI
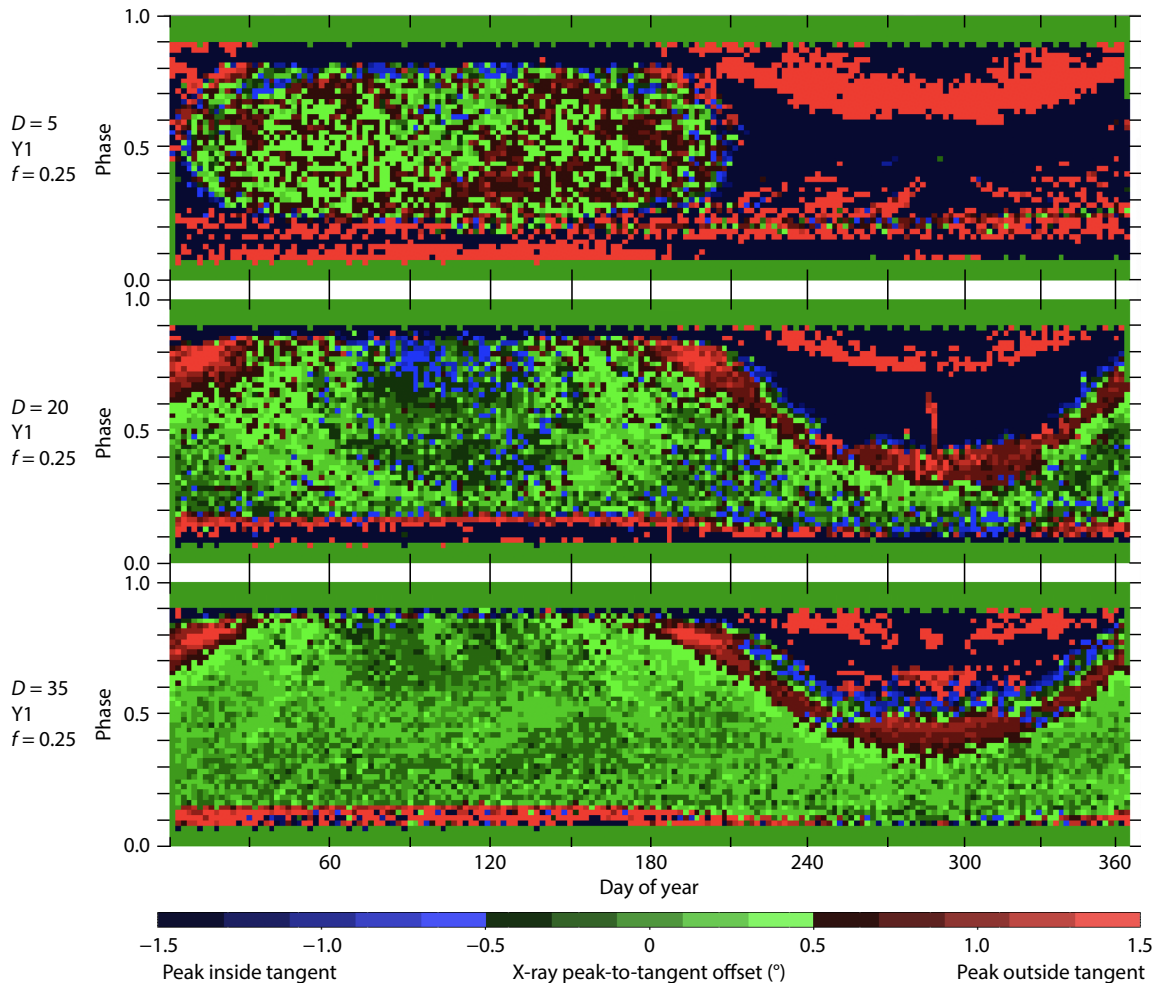
Figure 11. As for Figure 9, but for year 1 (Y1) and using the $f = 0.25$ magnetopause models generated from the appropriate cube data, and using the (top) $D = 5$, (middle) $D = 20$, and (bottom) $D = 35$ cm^{-3} X-ray emissivity cubes.

indeed be seen as sometimes reasonably true, but only for certain conditions, assumptions, models, and orbital positions or times. Some of these factors are linked and point to the same issue: that of geometry and whether the spacecraft is fully enough outside the magnetopause to be able to see or measure the tangent successfully. This is (partly) a seasonal effect, based on the orbit of the spacecraft (e.g., the spacecraft is usefully outside the magnetopause during almost all of a dayside-apogee orbit), but it is often problematically inside the magnetopause during much of a nightside-apogee orbit.

But there are also complications besides this in terms of the solar wind state (here, its density) affecting what one is trying to measure and disturbing the validity of assumptions that can be made. As an example, consider an observation taken during December, at apogee, during which the position of the peak in the X-ray emission can be successfully measured. The question is whether this position then aligns with the tangent to the magnetopause. Referring to Figure 11, then, *if* the solar wind is in a high-density state, and the magnetopause is then compressed somewhat inward (remember that the magnetopause position is unknown and is what SMILE-SXI is trying to measure), then conditions are such that the hypothesis can reasonably be assumed. However, *if* the solar wind is in fact in a low-density state, and the

magnetopause sits farther away from the Earth (although we are unaware of this), then the hypothesis cannot be safely assumed, and incorrect conclusions would result if the hypothesis were taken as being valid. In the case of SMILE, we should be partly helped because the onboard LIA, if working correctly and simultaneously, should be able to determine the current state of the solar wind.

It may be possible then that the same measured X-ray peak could be due to either case, a hypothesis-valid case or a hypothesis-invalid case, without knowing which it is. To help us here, though, we can refer to Figures 9 to 12 as general "maps" as to when in the SMILE mission and when in the SMILE orbit it is safest to conclude that the hypothesis is valid. For instance, as a counterexample to the preceding case, such as if we are able to measure the X-ray peak from a February apogee observation, then, again referring to Figure 11, the conditions are such that the hypothesis is reasonably valid whatever the solar wind conditions are.

This conclusion, however, brings up another issue: that of where exactly *this* magnetopause is. Or rather, if we conclude (e.g., from using the aforementioned maps) that the conditions are such that we are able to use the peak-to-tangent hypothesis to find the magnetopause position, we need to know precisely which

Read A.: Alignment of the magnetosheath X-ray peak with the magnetopause tangent as viewed by SMILE-SXI
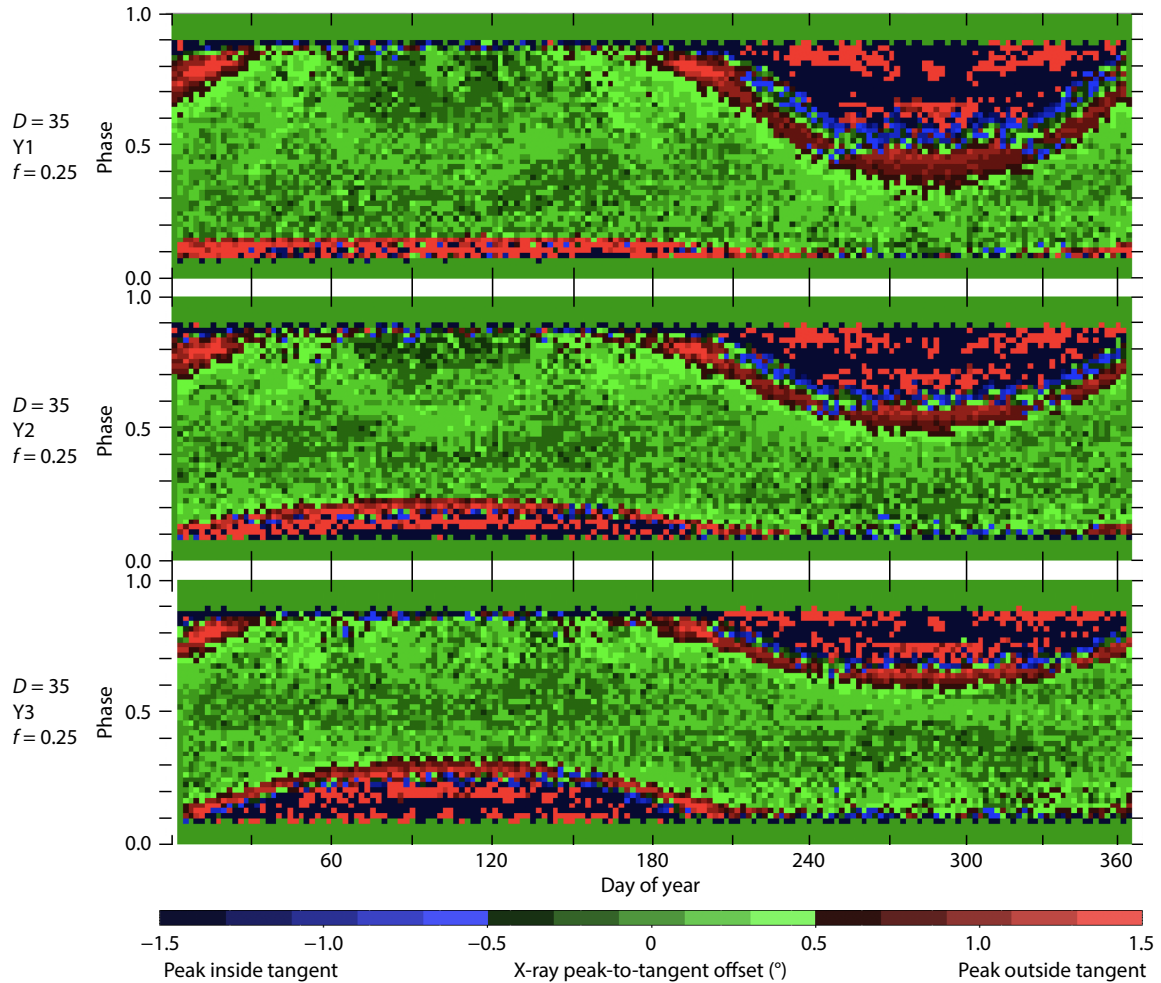
Figure 12. The same as for Figure 9, but for the $D = 35$ cm^{-3} X-ray emissivity cube and using the $f = 0.25$ magnetopause model, generated from the $D = 35$ cm^{-3} X-ray emissivity cube, and for (top panel) year 1 (Y1), (middle panel) year 2 (Y2), and (bottom panel) year 3 (Y3).

Table 3. Percentage of SXI ON time that the peak-to-tangent match is "good" (i.e., the magnitude of the offset angle is less than 0.5°) for various combinations of mission year (1–3), magnetopause (MP) surface model (max Lx, max dLx, $f = 0.25$), and X-ray emissivity cube model ($D = 5, 20, 35$ cm^{-3}).

Year	MP surface	$D = 5$	$D = 20$	$D = 35$
1	Max dLx	8.57	34.59	55.22
1	$f = 0.25$	17.45	48.42	68.84
1	Max Lx	6.18	0.37	3.10
2	$f = 0.25$	16.80	51.29	69.58
3	$f = 0.25$	15.67	50.08	69.17

Table 4. Percentage of SXI ON time that the peak-to-tangent match is "excellent" (i.e., the magnitude of the offset angle is less than 0.1°) for various combinations of mission year (1–3), magnetopause (MP) surface model (max Lx, max dLx, $f = 0.25$), and X-ray emissivity cube model ($D = 5, 20, 35$ cm^{-3}).

Year	MP surface	$D = 5$	$D = 20$	$D = 35$
1	Max dLx	0.10	0.47	1.09
1	$f = 0.25$	0.55	4.88	12.59
1	Max Lx	0.00	0.00	0.10
2	$f = 0.25$	0.48	5.47	13.16
3	$f = 0.25$	0.46	4.93	12.38

"magnetopause" has then been identified and positioned. The preceding analysis (and specifically Figures 9 and 10) concludes that the magnetopause surface that best fits the hypothesis method is the $f = 0.25$ model surface, that is, a surface that is neither where the emissivity begins to increase sharply (max dLx), nor where the emissivity is at a maximum (max Lx), but is an indistinct, less sharp surface lying somewhere in between the two. What may help here is the belief that the space between the max dLx surface and the max Lx surface (the dr in Figure 2), sometimes

referred to as the boundary layer, is artificially large in these modeled cubes created using magnetohydrodynamic (MHD) code (see Sun TR et al., 2019). Current codes are as yet unable to model the narrow width of the boundary layer sufficiently well, and in reality, the physical boundary layer (dr) is much narrower than the current models suggest. If this is the case, and the radial rise from approximately zero to maximum is very steep, then the max dLx, $f = 0.25$, and max Lx surfaces become nearly indistinguishable (i.e., they all occupy approximately the same space),

Read A.: Alignment of the magnetosheath X-ray peak with the magnetopause tangent as viewed by SMILE-SXI

Table 5. Percentages of year when various combinations of interplanetary magnetic field (B_Z), solar wind velocity (V_{SW}), and solar wind density (D_{SW}) values are observed, for the equivalent 3 years studied here from solar cycle 23 and solar cycle 24.[a]

B_Z (nT)	V_{SW} (km s^{-1})	D_{SW} (cm^{-3})	Solar cycle 23			Solar cycle 24		
			2000	2001	2002	2013	2014	2015
<−5	>400	>5	3.16	2.83	3.46	1.30	1.14	3.05
<−5	>400	>20	0.29	0.27	0.23	0.09	0.12	0.41
<−5	>400	>35	0.04	0.04	0.05	0.04	0.02	0.08
<−5	>400	<10	4.15	3.54	4.34	1.84	1.43	2.64
<−5	>400	15–25	0.41	0.31	0.31	0.14	0.17	0.42
<−5	>400	>25	0.16	0.14	0.12	0.07	0.06	0.24
<−2.5	>400	>5	5.68	5.13	6.82	2.98	3.16	6.48
<−2.5	>400	>35	0.06	0.06	0.08	0.04	0.03	0.09
<−5	300–500	>5	4.62	4.19	4.65	2.84	3.30	4.52
<−5	300–500	>35	0.04	0.05	0.11	0.04	0.02	0.18
<−2.5	300–500	>5	9.94	9.91	10.17	7.78	9.42	11.15
<−2.5	300–500	>35	0.06	0.12	0.15	0.05	0.05	0.25

[a]Rows 1−3 treat all the emissivity cube model values as restrictive limits. Rows 4−6 treat the solar wind density model values as being representative of a range of values. Rows 6−12 are equivalent to rows 1 and 3, but treating B_Z, V_{SW}, or both as being representative of a range of values. Percentages for other combinations of model ranges can be estimated from the table. A large scatter in percentage of the year is often seen for the same model combination (along a row).

and the question of where in the cube the appropriate magnetopause surface is situated becomes much simpler and unambiguous to define.

5.2 Simple Geometrical Considerations

The methods used in this paper, including the important points that the magnetopause surface is extracted directly from the X-ray emissivity cube and that both the surface and the emission through the cube are viewed from the POV of the spacecraft, can be streamlined to much simpler examples by using emissivity shapes and profiles and "magnetopause" surfaces that are far easier to understand. In fact, the problem reduces from a complex X-ray–magnetosheath problem to simple geometrical issues involving a simple volume of constant emission.

A much simpler scenario to consider first would be if the emission were purely from a thin hemispherical shell. A simple emissivity cube (called cube "C1") was constructed with constant emissivity in a hemispherical (positive GSE-X, i.e., Sun-facing) shell of width ±0.2 R_E at a radius (from the Earth) of 7.17 R_E and zero emissivity outside this shell. An accompanying representative ("magnetopause") surface — a simple hemispherical grid of radius 7.17 R_E — was also constructed. The SMILE OV simulator was again used to show the hemispherical surface and what is visible through the modeled C1 cube from the POV of the SMILE spacecraft, and then to again calculate the X-ray peak-to-tangent offset angle by using the single-revolution orbits discussed earlier. A near-apogee snapshot of the simulated view is shown in the left-hand panel of Figure 13. For this model, the peak in the emission and the tangent to the surface align very well (as shown in the left panel of Figure 13) for all times when the spacecraft is outside the shell; that is, for this simple model, the hypothesis that the apparent maximum in the X-ray emissivity aligns with the tangent to the

"magnetopause" is well met.

This model, however, is too simplistic and does not match what is observed in the much more realistic, modeled X-ray emissivity cubes used for the bulk of this work and created using the MHD code by Sun TR et al. (2019). To match these cubes more closely, a second cube ("C2") was constructed, this time with a thicker hemispherical shell of emission, with a radial form that rises quickly from zero to peak (the peak at 7.17 R_E) over 0.5 R_E, and then declines more slowly from peak to half of the peak over 1.7 R_E. A simulated snapshot using this C2 cube (and again the r = 7.17 R_E hemispherical "magnetopause" surface) is shown in the central panel of Figure 13. When this model with the thicker shell is used, the peak in the X-ray emission and the tangent to the magnetopause surface are shown to align very well again (this is discussed further in the subsequent paragraphs). That is, when this more realistic (although still simple) model is used, one sees that the hypothesis is still well met.

Again, though, this is not the whole story because the true magnetosheath is not believed to be cylindrically symmetrical or to be constantly bright over all theta (the angle away from the GSE-X axis) and all phi (the angle around the GSE-X axis). The magnetosheath is much brighter nearer the nose (at small theta) than far from the nose (at large theta), and phi has large variations, largely due to the bright cusps, but also far from the cusps, where large discrepancies are seen between the horizontal (X-Y) and vertical (X-Z) planes. An extreme example of the first of these (brighter at small theta, fainter at large theta) is shown in the right-hand panel of Figure 13, where the modeled X-ray emissivity cube ("C3") is made up of only a small cubic volume (0.2 R_E across) of constant emissivity at the position of the nose (X = 7.17 R_E, Y = Z = 0), and zero emissivity elsewhere. In this admittedly extreme example, the peak in the X-ray emission is almost always
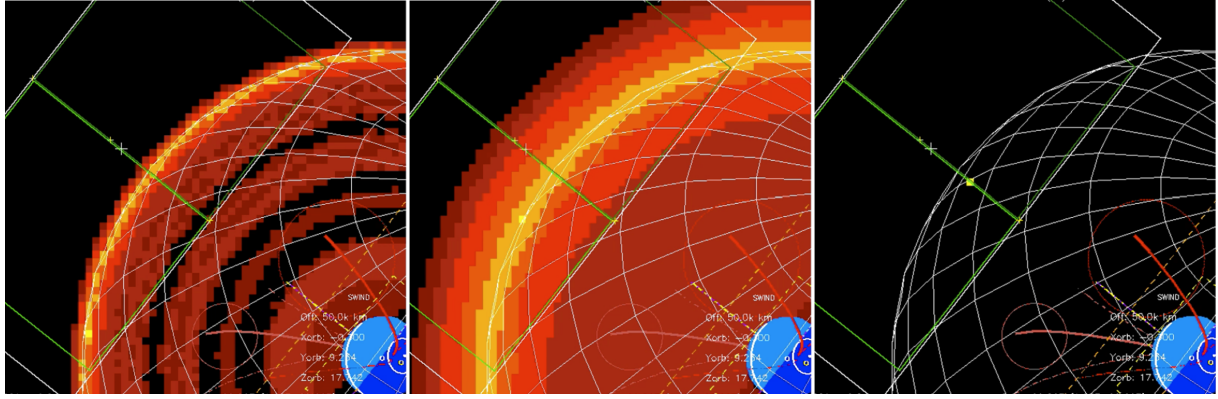
Figure 13.   Views from the POV of the SMILE spacecraft (features as described in Figure 3) of three simple X-ray emissivity cube models: (left, C1) a thin hemispherical shell (at 7.17 R_E, with a width of ±0.2 R_E) of constant emissivity, (center, C2) a thicker hemispherical shell, with a peak at 7.17 R_E, and with a sharp rise to this radius (zero to peak over 0.5 R_E), and a slower decline outside (peak to 0.5 peak over 1.7 R_E), (right, C3) a small cube (0.2 R_E across) of constant emissivity at $X = 7.17$ R_E ($Y = Z = 0$). The gridded (magnetopause) surface is (in all the cases) a hemisphere of radius 7.17 R_E. The SXI optic FOV (white rectangle) is 32.09° × 15.85°, which gives the angular scale of the image. The spacecraft is at a position of GSE = [−0.30, 9.25, 17.74] R_E.
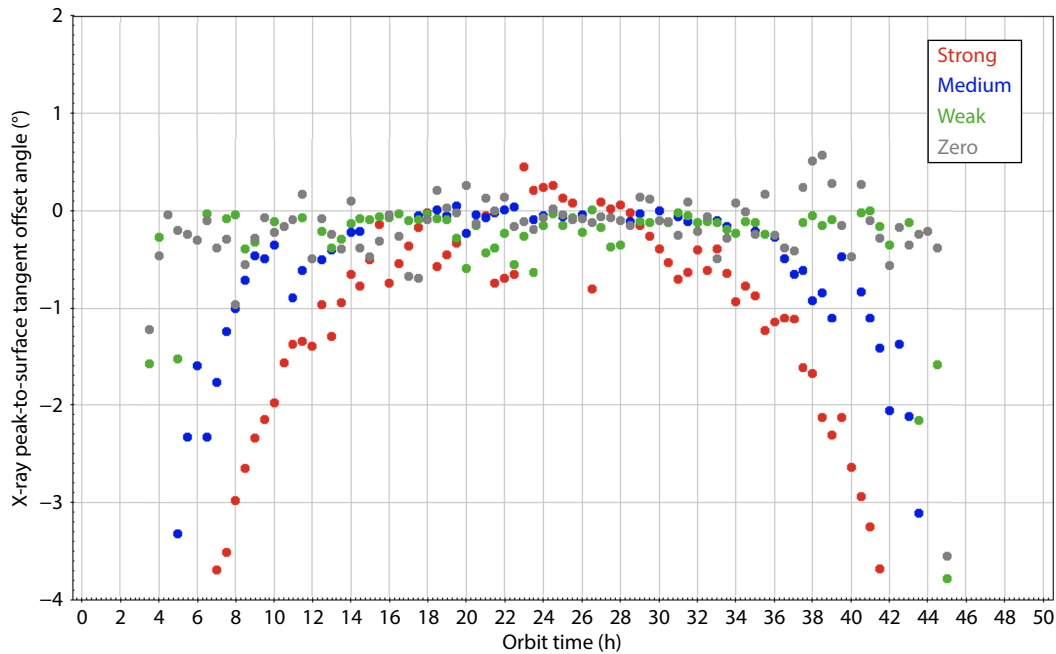
Figure 14.   The X-ray peak-to-tangent angular offset (y-axis, degrees) versus time (x-axis, hours), using the hemispherical shell model with a thicker width (the C2 cube) for the X-ray emission described in the text and shown in the central panel of Figure 13, but with various gradients applied (strong, medium, weak, and zero [no gradient]; for details, see the color key and text) such that the emissivity decreases (or does not, in the zero-gradient case) as the distance away from the x-axis is increased. The dusk-apogee single-revolution orbit, discussed previously, is used throughout, and again the $r = 7.17$ R_E hemispherical "magnetopause" surface is used.

seen (as in the right panel in Figure 13) to be significantly inside the tangent to the magnetopause surface (again the $r = 7.17$ R_E hemisphere). In fact, it is only when the spacecraft is at an X-position of 7.17 R_E that the X-ray peak and the tangent to the magnetopause do align. If the spacecraft is not within the $X = 7.17$ plane, then the peak lies inside the tangent and the hypothesis is not met.

Although this is an extreme example, the true magnetosheath is believed to have significant variations in the radial emissivity profile with theta (and with phi), and this assumption was

explored further. Further X-ray emissivity cubes were constructed, with a starting form identical to the C2 cube (i.e., the thicker hemispherical shell model described above and shown in the middle panel of Figure 13), but with various different gradients (strong, medium, weak, and zero [no gradient]) applied such that the emissivity decreases (or does not, in the zero-gradient case) as the distance away from the X-axis is increased. Specifically, the emissivity at a point (X, Y, Z) is reduced by an amount of $E_{nose} \times \sqrt{Y^2 + Z^2}/L$, where E_{nose} is the emissivity at the nose, and L is 2, 5, and 8 R_E for the strong, medium, and weak cases, respectively (the

emissivity remains at zero beyond the boundary, where the emissivity is reduced to zero). Figure 14 shows, as in previous figures, the X-ray peak-to-tangent angular offset (*y*-axis, degrees) versus time (*x*-axis, hours), using these "gradient" cubes (and again using the $r = 7.17$ R_E hemispherical "magnetopause" surface) in the OV simulator, and using only the single-revolution dusk-apogee orbit used previously. The various colors show the gradient used.

Looking first at the zero-gradient (gray) case, this case is identical to the C2 cube, and as discussed previously, it behaves very well, with a near-zero offset angle for most of the orbit. When gradients are introduced to mimic the emission being stronger nearer the nose than far from the nose, then deviations away from zero offset (when the hypothesis is then not met) are seen. When stronger gradients are introduced (and the emission becomes more nose-peaked and flank-weakened, then the deviations away from zero offset become larger. This simple change to the emission profile, to make it stronger nearer the nose, is only one example of how a small deviation from a uniform emission profile can lead to a nonzero peak-to-tangent offset.

When these simple considerations are taken into account, because the X-ray emission within the true magnetosheath is so spatially complex, it is perhaps no surprise that deviations away from a simple zero offset between the X-ray peak and the tangent to the magnetopause are often seen, and indeed are expected.

5.3 Utility of the Results

The question is whether these possible offsets between the X-ray peak and the magnetopause tangent are important or significant as regards SMILE-SXI specifically. For a typical distance of SMILE at apogee away from the magnetopause of 18 R_E, then an offset of 1° (e.g., see Figures 4 and 5) corresponds to a physical offset of size 0.31 R_E. We then need to ask how 0.31 R_E compares with what SXI is able to and is aiming or designed to achieve.

The software simulator SXI_SIM (see Sembay et al., 2024) uses modules of the OV simulator (see Section 2.1) and other code to predict the foreground magnetospheric SWCX emission and the background emission that SXI might observe in orbit. For an input spacecraft position and viewing direction, the expected foreground and background components are calculated, and the photon components are passed through the full SXI instrument response, after which they are all combined to yield the estimated total counts in the SXI FOV. Poisson noise is added to the total counts, and the background is subtracted to leave the estimated foreground SWCX emission with the appropriate noise. Last, instrumental vignetting is applied to yield an image of the expected foreground emission for a user-defined integration time.

Various MHD X-ray emissivity cubes (including those in this paper) can be used as inputs, and output images for various integration times can be analyzed to calculate the spatial accuracy to which the subsolar magnetopause location, $R0_{MP}$, can be determined. It can be estimated (Sembay et al., 2024; Sembay, private comm.) that, for a 5-min integration time and using the $D = 20$ emissivity cube, then for observations near apogee, the error in $R0_{MP}$ is approximately 0.3 R_E. When using the $D = 35$ emissivity cube and again a 5-min integration time, then the error in $R0_{MP}$ is 0.2 R_E.

These values are quite comparable to the physical peak-to-tangent offset shift discussed at the beginning of this section. Usage of the $D = 5$ emissivity cube (and a 5-min integration time) yields a much larger error in $R0_{MP}$, ~2.5 R_E, and even a 20-min integration time reduces the error in $R0_{MP}$ to only ~1.3 R_E.

The formal science requirements for the SXI state that the subsolar magnetopause location, $R0_{MP}$, should be derivable to a spatial accuracy better than 0.5 R_E for a solar wind flux $\geq 4.9 \times 10^8$ cm^{-2} s^{-1} and an SXI integration time of 5 min. The 0.31 R_E physical peak-to-tangent offset shift discussed previously makes up a large fraction of this accuracy limit. The $D = 20$ and $D = 35$ emissivity cubes have solar wind fluxes (8×10^8 cm^{-2} s^{-1} and 14×10^8 cm^{-2} s^{-1}, respectively) above the flux limit, whereas the $D = 5$ emissivity cube has a solar wind flux (2×10^8 cm^{-2} s^{-1}) below the flux limit.

6. Conclusions

An idea — a hypothesis — has been suggested that, from the POV of a suitably positioned spacecraft, the apparent peak in the magnetosheath X-ray intensity should align with the tangent to the magnetopause. Although this hypothesis may indeed be applicable in simple scenarios, its applicability in more complex, perhaps more real-world, situations may not be so clear-cut.

The SXI on board the SMILE spacecraft (due for launch into a high-altitude orbit in 2025) will be able to view the Earth's magnetosheath in soft X-rays. Using the SMILE mission orbit, together with MHD simulations of the expected X-ray emissivity of the Earth's magnetosheath, simulated images of the X-ray emission and the pseudo-magnetopause geometry (formed from the locations where the X-ray emissivity, or the gradient in X-ray emissivity, peaks) from the POV of SMILE-SXI have been constructed. These images are able to address the validity of this hypothesis.

It was shown that, for good agreement with the peak-to-tangent hypothesis to occur, the spacecraft needs to be sufficiently well positioned, well outside of the magnetopause, to be able to clearly see both the magnetosheath and the tangent to the magnetopause. There are orbital aspects to this: low-altitude times near perigee are not good because the spacecraft is not outside the magnetopause. There are also seasonal aspects: orbits with dayside apogees, for instance, are generally very good because the spacecraft travels out sunward at high altitude, and excellent views of the magnetopause are obtained. But a half-year later, during nightside-apogee orbits, the spacecraft travels behind the Earth and only rarely exits the magnetopause. Dusk-apogee and dawn-apogee orbits are intermediate and mirror each other in behavior. In addition, changes are seen over the SMILE mission; for example, the dayside-apogee orbits worsen slightly over the first 3 years of the mission, whereas the nightside-apogee orbits improve slightly. Additionally, it was shown that many more times of good agreement with the peak-to-tangent hypothesis occur when the solar wind is in a high-density (as opposed to a low-density) state. Here, the magnetopause is compressed, and the spacecraft is more often a good distance outside the magnetopause to be able to view the magnetosheath and magnetopause sufficiently well. Furthermore, it was shown that, for the X-ray emissivity models used here, which may have a boundary layer (between where the emissivity gradient peaks and

where the emissivity itself peaks) that is unnaturally wide, a magnetopause surface that follows neither where the emissivity gradient peaks nor where the emissivity itself peaks, but somewhere in between these two surfaces (and closer to the former), is a magnetopause surface that better matches the peak-to-tangent hypothesis.

Acknowledgments

References

Branduardi-Raymont, G., Wang, C., Escoubet, C. P., Adamovic, M., Agnolon, D., Berthomier, M., Carter, J. A., Chen, W., Colangeli, L., … Zhu. Z. (2018). SMILE definition study report. *European Space Agency*, *ESA/SCI*, 1. https://doi.org/10.5270/esa.smile.definition_study_report-2018-12

Branduardi-Raymont, G., and Wang, C. (2022). The SMILE mission. In: C. Bambi et al. (Eds.), *Handbook of X-ray and Gamma-ray Astrophysics* (pp. 1–22). Singapore: Springer. https://doi.org/10.1007/978-981-16-4544-0_39-1

Collier, M. R., and Connor, H. K. (2018). Magnetopause surface reconstruction from tangent vector observations. *J. Geophys. Res.: Space Phys.*, *123*(12), 10189–10199. https://doi.org/10.1029/2018JA025763

Connor, H. K., Sibeck, D. G., Collier, M. R., Baliukin, I. I., Branduardi-Raymont, G., Brandt, P. C., et al. (2021). Soft X-ray and ENA imaging of the Earth's dayside magnetosphere. *J. Geophys. Res.: Space Phys.*, *126*, e2020JA028816. https://doi.org/10.1029/2020JA028816

Jorgensen, A. M., Sun, T. R., Wang, C., Dai, L., Sembay, S., Wei, F., Guo, Y. H., and Xu, R. L. (2019). Boundary detection in three dimensions with application to the SMILE mission: The effect of photon noise. *J. Geophys. Res.: Space Phys.*, *124*(6), 4365–4383. https://doi.org/10.1029/2018JA025919

Robertson, I. P., Collier, M. R., Cravens, T. E., and Fok, M. C. (2006). X-ray emission from the terrestrial magnetosheath including the cusps. *J. Geophys. Res.: Space Phys.*, *111*(A12), A12105. https://doi.org/10.1029/2006JA011672

Roelof, E. C., and Sibeck, D. G. (1993). Magnetopause shape as a bivariate function of interplanetary magnetic field B_z and solar wind dynamic pressure. *J. Geophys. Res.: Space Phys.*, *98*(A12), 21421–21450. https://doi.org/10.1029/93JA02362

Samsonov, A., Carter, J. A., Read, A., Sembay, S., Branduardi-Raymont, G., Sibeck, D., and Escoubet, P. (2022a). Finding magnetopause standoff distance using a soft X-ray imager: 1. Magnetospheric masking. *J. Geophys. Res.: Space Phys.*, *127*(12), e2022JA030848. https://doi.org/10.1029/2022JA030848

Samsonov, A., Sembay, S., Read, A., Carter, J. A., Branduardi-Raymont, G., Sibeck, D., and Escoubet, P. (2022b). Finding magnetopause standoff distance using a soft X-ray imager: 2. Methods to analyze 2-D X-ray images. *J. Geophys. Res.: Space Phys.*, *127*(12), e2022JA030850. https://doi.org/10.1029/2022JA030850

Sembay, S., Alme, A. L., Agnolon, D., Arnold, T., Beardmore, A., Belén Balado Margeli, A., Bicknell, C., Bouldin, C., BranduardiRaymont, G., … Yang, S. (2024). The Soft X-ray Imager (SXI) on the SMILE Mission. *Earth Planet. Phys.*, *8*(1), 5–14. https://doi.org/10.26464/epp2023067

Shue, J. H., Song, P., Russell, C. T., Steinberg, J. T., Chao, J. K., Zastenker, G., Vaisberg, O. L., Kokubun, S., Singer, H. J., … Kawano, H. (1998). Magnetopause location under extreme solar wind conditions. *J. Geophys. Res.: Space Phys.*, *103*(A8), 17691–17700. https://doi.org/10.1029/98JA01103

Sun, T. R., Wang, C., Connor, H. K., Jorgensen, A. M., and Sembay, S. (2020). Deriving the magnetopause position from the soft X-ray image by using the tangent fitting approach. *J. Geophys. Res.: Space Phys.*, *125*(9), e2020JA028169. https://doi.org/10.1029/2020JA028169

Sun, T. R., Wang, C., Sembay, S. F., Lopez, R. E., Escoubet, C. P., Branduardi-Raymont, G., Zheng, J. H., Yu, X. Z., Guo, X. C., … Guo, Y. H. (2019). Soft X-ray imaging of the magnetosheath and cusps under different solar wind conditions: MHD simulations. *J. Geophys. Res.: Space Phys.*, *124*(4), 2435–2450. https://doi.org/10.1029/2018JA026093

Sun, T. R., Wang, X., and Wang, C. (2021). Tangent directions of the cusp boundary derived from the simulated soft X-ray image. *J. Geophys. Res.: Space Phys.*, *126*(3), e2020JA028314. https://doi.org/10.1029/2020JA028314

Read A.: Alignment of the magnetosheath X-ray peak with the magnetopause tangent as viewed by SMILE-SXI